Depth and Rate of Fading on Fixed Wireless Channels between 200 MHz and 2 GHz in Suburban Macrocell Environments

Kyle N. Sivertsen, *Graduate Student Member, IEEE*, Anthony Liou and David G. Michelson, *Senior Member, IEEE*

Abstract— Various bands between 200 MHz and 2 GHz have recently been reallocated to multipoint fixed wireless services. The links in such systems are usually obstructed by buildings and foliage and are susceptible to fading caused by windblown trees and foliage. To date, there have been relatively few efforts to characterize either the depth of fading in bands below 1.9 GHz or the rate of fading in any of these bands. We transmitted CW signals in the 220, 850 and 1900 MHz bands from a transmitter located 80 m above ground level in a typical suburban macrocell environment and collected time-series of received signal strength at distances between 1 and 4 km from the site. We reduced the data to show how the depth and rate of fading depend on the frequency band, time-averaged wind speed and distance in such an environment. Our most significant finding is that the rate of signal fading is very similar in all three bands. In particular, it is not proportional to carrier frequency, as a simplistic model involving moving scatterers might suggest. These results will provide useful guidance to those who seek to simulate, or develop detailed physical models of, fade dynamics in such environments.

***Index Terms*— channel model, fading channels, macrocell environment, radiowave propagation, radiowave propagation – meteorological factors**

I. Introduction

In recent years, as: (i) common carriers seek methods for providing either fixed or nomadic network access services to residential households without the expense of deploying wireline connectivity over the last mile [1],[2] and (ii) public utilities seek methods that will allow them to: (a) detect and report outages, (b) monitor usage, and (c) implement strategies that encourage customers to limit consumption and adopt sustainable practices [3]-[5], the possibility of deploying fixed wireless multipoint communication systems in suburban macrocell environments has attracted considerable interest. In order to provide developers with the insights required to design effective systems, several groups in Canada, the United States, the United Kingdom, Chile, Australia and elsewhere have conducted measurement campaigns which have aimed to characterize the depth of signal fading observed in such environments, *e.g.*, [6]-[13].

In macrocell environments, the base station antenna is mounted well above the local rooftop or treetop level and the remote terminal antenna is mounted below the local rooftop or treetop level. As a result, the wireless links are usually obstructed by intervening obstacles and a large fraction of the signal that reaches the receiver does so as a result of scattering and diffraction by objects in the environment. Because both the transmitting and receiving antennas in such applications are fixed, signal fading is caused solely by the motion of objects in the environment that scatter and diffract the signal. In suburban macrocell environments, a large fraction of those objects are trees and foliage with leaves and branches that sway when blown by the wind.

The vast majority of previous studies of fixed wireless channels in suburban macrocell environments focused on individual frequency bands at 1.9 GHz and above, including the PCS band at 1.9 GHz, the ISM band at 2.45 GHz, the Fixed Wireless Access (FWA) band at 3.5 GHz and the U-NII and ISM bands at 5.2 and 5.8 GHz. However, spectrum regulators have recently begun to reallocate frequency bands below 2 GHz in order to help meet the requirements for broadband wireless access for urban and rural areas and/or narrowband telemetry for public utilities. In Canada, spectrum in frequency bands near 700 MHz has been proposed for fixed wireless broadband use in rural areas [18] and may find application in distribution automation by the electrical power industry. Frequency bands such as 220–222 MHz, 1429.5–1432 MHz and 1800–1830 MHz have recently been designated for utility telemetry and distribution automation [19]. Regulators are increasingly designating multiple primary allocations within individual frequency bands, as well as proposing more flexible licensing schemes, in an attempt to accommodate different users and services in the same

Manuscript received April 16, 2009; revised February 27, 2010; accepted March 31, 2010.

K .N. Sivertsen and D. G. Michelson are with the Radio Science Laboratory, Department of Electrical and Computer Engineering, University of British Columbia, Vancouver, BC, Canada, V6T 1Z4 (e-mail: {ksiverts, davem}@ece.ubc.ca).

A. E.-L. Liou was with the Radio Science Laboratory at the University of British Columbia. He is currently with Universal Scientific Industrial Co., Taiwan. (e-mail: eliou@ece.ubc.ca)

This work was supported in part by grants from Bell Canada, British Columbia Hydro and Power Authority, Tantalus Systems and Western Economic Diversification Canada.

Digital Object Identifier

spectrum. Both the amount of radio spectrum, and the choice of frequency bands available for fixed wireless use, will almost certainly increase in coming years.

The manner in which path loss, or its reciprocal, path gain, is affected by the carrier frequency, the heights of and separation between the base station and mobile terminal in suburban macrocell environments over the range from 200 MHz to 2 GHz has been well-studied over the years and has been captured by several standard models [20]-[22]. However, existing channel models do not provide a description of either the depth or rate of signal fading that fixed wireless channels will experience over this frequency range in suburban macrocell environments. Although previous efforts to characterize the fade dynamics of propagation through vegetation provided useful insights, the amount of data collected was limited [23]-[25].This lack of information places those charged with planning, simulating or deploying fixed wireless systems in suburban macrocell environments at a severe disadvantage when asked to predict the performance of data link protocols (including handshaking schemes) and opportunistic schedulers that attempt to synchronize transmission with favourable channel conditions.

Here, we take the first steps to determine how both the depth and rate of fading on fixed wireless channels in a typical suburban macrocell environment vary with carrier frequency, wind speed and distance across the frequency range from 200 MHz to 2 GHz. We established a transmitting site atop an eighteen-storey office tower located in the middle of a large suburban area. We simultaneously broadcast single carrier signals in the 220, 850 and 1900 MHz bands and collected time-series of the received signal strength observed in each band at fixed locations at ranges between 1 and 4 km. The frequencies that we employed bracket the majority of the bands that have been allocated to fixed wireless access and SCADA (supervisory control and data acquisition) applications. Although our results strictly apply to narrowband channels, they are also relevant to single carriers in multicarrier modulation schemes.

The remainder of this paper is organized as follows: In Section II, we discuss common representations of fading on fixed wireless channels. In Section III, we summarize the essential aspects of our second-order model of fading on narrowband channels. In Section IV, we describe our measurement setup and test site. In Section V, we present our results and suggest how these results can be used in system-level simulations. In Section VI, we summarize our findings and contributions and discuss the implications of our results.

II. Signal Fading on Fixed Wireless Channels

Because fading on fixed wireless channels in macrocell environments normally follows a Ricean distribution, the depth of fading is typically expressed in terms of the Ricean K-factor. The rate at which signal fading occurs may be characterized either by the Level Crossing Rate (LCR) and Average Fade Duration (AFD) at selected thresholds above and below the mean signal strength [13] (which depend on both the first- and second-order statistics of the fading signal) or by a Doppler power spectrum [14],[15] (which depends only upon the second-order statistics). Although the latter representation is particularly useful because it is a key input for algorithms used to simulate (or emulate) fading channels, *e.g.*, [16],[17], estimation of the Doppler power spectrum from measured data generally requires coherent time series data (amplitude and phase). Fading on fixed wireless links occurs so slowly, however, that lack of phase coherence between the local oscillators in the widely separated transmitter and receiver can severely distort the measurement. Although a method for estimating the Doppler spectrum from amplitude-only measurement data was proposed in [15], it is mainly intended for use on short-range line-of-sight paths where the Ricean K-factor is high, *e.g.*, $K > 10$, and is much less effective in suburban macrocell environments where K is often < 10.

In [13], it was found that the measured level crossing rate (LCR) and/or average fade duration (AFD) distributions seen on fixed wireless links can be fitted to expressions that are normally justified only for mobile wireless links. This allows one to express the time variation on the link in terms of just three parameters: the mean signal strength, the Ricean K-factor, and an effective maximum Doppler frequency which is referred to as $f_{d,FW}$ in [13] and which we will simply refer to as f_d. The details are described in the next section.

III. A Second-Order Fading Channel Model

If the complex envelope of the time-varying path gain, $g(t)$, experienced by either a mobile or fixed links is given by the sum of a fixed component V and a zero-mean complex Gaussian process $v(t)$ and $r(t) = |g(t)|$, the first-order statistics of r will follow a Ricean distribution where

$$p(r) = \frac{2(K+1)r}{G} \exp\left(-K - \frac{(K+1)r^2}{G} \right) \cdot I_0\left(2\sqrt{\frac{K(K+1)}{G}} r \right), \quad (1)$$

G is the average envelope power and $I_0(\cdot)$ is the zero order modified Bessel function of the first kind. In such cases, the Ricean K-factor is given by

$$K = |V|^2 \Big/ \overline{|v(t)|^2} = |V|^2 / \sigma^2 , \quad (2)$$

where σ^2 is the power in the time-varying component. Various methods for estimating K have been proposed. Here, we use the moment-based method described in [26] where

$$K = \frac{|V|^2}{\sigma^2} = \frac{\sqrt{G^2 - \sigma_G^2}}{G - \sqrt{G^2 - \sigma_G^2}} , \quad (3)$$

and σ_G is the rms fluctuation of the envelope about G, *i.e.*, the standard deviation of $|g(t)|^2$.

In cases where the base station is fixed, the terminal is in motion, and scattering is two-dimensional and isotropic, the

Doppler spectrum of the time-varying component is given by Clarke's U-shaped spectrum and ranges from $-f_{d,\max}$ to $f_{d,\max}$. The frequency offset of the carrier that corresponds to the fixed component is determined by the direction of the propagation path relative to the velocity of the terminal. In such cases, the LCR and AFD are given by

$$LCR = \sqrt{2\pi(K+1)} f_d \rho \cdot \exp\left(-K-(K+1)\rho^2\right) \cdot I_0\left(2\sqrt{K(K+1)}\rho\right) \quad (4)$$

and

$$AFD = \frac{\Pr(r<T)}{LCR} = \frac{\left(1-Q\left(\sqrt{2K},\sqrt{2(K+1)\rho^2}\right)\right)\exp\left(K+(K+1)\rho^2\right)}{\sqrt{2\pi(K+1)} f_d \rho I_0(2\sqrt{K(K+1)}\rho)}, \quad (5)$$

where T is the threshold voltage, $\rho = T/r_{rms}$ is the threshold normalized to the rms envelope, $Q(\cdot)$ is the Marcum-Q function and, in this case, f_d corresponds to $f_{d,\max}$ [13].

In cases where both the base station and the terminal are fixed, time variation is entirely due to the motion of scatterers in the environment and the corresponding Doppler spectrum generally exhibits a sharp peak at the carrier frequency and rapidly decays as the frequency offset increases, *e.g.*, [14]. In [13], it was shown that for cases where the time derivative of the envelope $\dot{r}$ is independent of r, the expressions for LCR and AFD given in (4) and (5) do not depend on the shape of the Doppler spectrum. In particular, applying the value of K estimated using (3) to the expressions for LCR and AFD given by (4) and (5), and choosing an appropriate value for f_d will often provide a good approximation to the LCR and AFD characteristics observed on fixed wireless links. Further, it was reported that a good estimate of f_d can often be obtained by considering only the Zero Crossing Rate, ZCR, which is defined as the value of LCR for $\rho = 1$, *i.e.*,

$$\text{ZCR} = \sqrt{2\pi(K+1)} f_d \exp\left(-2K-1\right) \cdot I_0\left(2\sqrt{K(K+1)}\right). \quad (6)$$

For $K > 3$, this expression is virtually insensitive to the actual value of K, yielding the convenient approximation

$$f_d \approx 1.4\,\text{ZCR}. \quad (7)$$

The significance of f_d is now less clear given that it no longer applies to the maximum frequency component of Clarke's U-shaped spectrum. In Section IV-B, we recount a possible interpretation of the physical significance of f_d. In the sections that follow, we describe our efforts to characterize the depth and rate of fading experienced over fixed wireless links across a broad frequency range from 200 MHz to 2 GHz in a typical suburban macrocell environment.

IV. The Measurement Setup

A. Tri-band Channel Sounder

Our tri-band channel sounder consists of three continuous wave (CW) transmitters and three corresponding receivers that operate in the 220, 850 and 1900 MHz frequency bands. A block diagram of the CW transmitter is shown in Figure 1(a). The signal source portion of the transmitter contains a pair of Marconi 2022 RF signal generators, each of which is capable of supplying a CW signal up to 6 dBm over the range 10 kHz to 1 GHz, and a Marconi 2031 RF signal generator capable of supplying a CW signal up to 13 dBm over the range 10 kHz to 2.7 GHz. The signal generators are locked to a 10 MHz reference signal supplied by a Stanford Research Systems PRS10 Rubidium frequency standard. It, in turn, is disciplined by the 1 pulse per second (PPS) signal supplied by a Trimble Resolution-T GPS receiver that has been designed for such applications.

The amplifier portion contains three power amplifiers: (i) a TPL Communications LMS series RF power amplifier capable of delivering between 20 and 100 W at 220 MHz, (ii) a Unity Wireless Dragon RF power amplifier capable of delivering up to 30 W between 869 and 894 MHz and (iii) a Unity Wireless Grizzly RF power amplifier capable of delivering up to 35 W

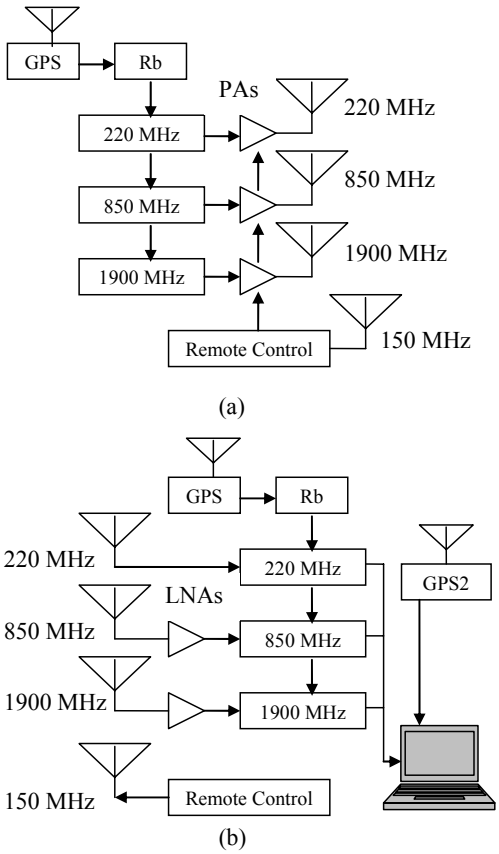

Fig. 1. (a)The tri-band transmitter that was deployed at the base station and (b) the tri-band receiver that was carried aboard the propagation measurement van.

TABLE I
LINK BUDGET PARAMETERS FOR THE TRI-BAND CHANNEL SOUNDER.

Parameter	220 MHz	850 MHz	1900 MHz
Transmitted Power	43 dBm	43 dBm	43 dBm
Transmit Cable Loss	1.3 dB	2.7 dB	4.3 dB
Transmit Antenna Gain	8.1 dBi	6.1 dBi	5 dBi
Receive Antenna Gain	1 dBi	1 dBi	1 dBi
Receive Cable Loss	0.37 dB	0.76 dB	1.2 dB
Receiver LNA Gain	-	30 dB	26 dB

between 1930 and 1990 MHz. During data collection, all three amplifiers were configured to deliver 20 W signals to their respective feedlines. A wireless remote control device that operates near 150 MHz allowed the data collection team to remotely enable or disable the power amplifiers at the start or end of a measurement session. The 220, 850 and 1900 MHz transmitting antennas are omnidirectional and have gains of 8.1, 6.1 and 5.0 dBi, respectively. The remaining parameters used in the system link budget for each band are given in Table I.

A block diagram of our multiband receiver is shown in Figure 1(b). The receiving antennas are omnidirectional and all have the same nominal gain of 1 dBi. When used in NLOS configurations, fixed wireless antennas are typically mounted at heights between 0.5 m (*e.g.*, for nomadic applications) and 4 m (*e.g.*, for permanent installations). As a compromise, we mounted the antennas on the roof of our propagation measurement van at a height of 2.3 m.

The multiband receiver consists of: (i) a pair of Anritsu MS2651B spectrum analyzers that operate over the range from 9 kHz to 3 GHz with a selectable IF bandwidth, (ii) an Anritsu MS2721A spectrum analyzer that operates over the range from 100 kHz to 7.1 GHz with a selectable IF bandwidth, (iii) a Stanford Research Systems PRS10 Rubidium frequency standard that generates a 10 MHz reference signal to which the spectrum analyzers can be locked and (iv) a Trimble Resolution-T GPS receiver that supplies the 1 PPS signal used to discipline the frequency standard. External low-noise pre-amplifiers with 30 dB and 26 dB gain were used to increase the sensitivity of the spectrum analyzers that measure the received strength of the 850 and 1900 MHz signals, respectively. We used a laptop computer equipped with a GPIB adapter to: (i) configure the spectrum analyzers and (ii) collect data from them. We geocoded the data with a nominal circular error probability (CEP) of less than 5 metres using location information supplied by a u-blox Antaris 4 SuperSense GPS receiver.

B. *Verification Protocol*

Before we collected any field data, we verified the function and operation of our tri-band CW channel sounder using a Spirent SR5500 channel emulator. We set the relevant narrowband channel parameters, including path gain and Ricean K-factor, to various values over a broad range and, in each case, confirmed that we were able to correctly estimate each of the parameters. We verified the transmitted power levels using a Bird Model 5000EX digital wattmeter.

C. *Weather Instruments*

We measured the wind speed, wind direction, rain rate and outdoor temperature using a Davis Vantage Pro 2 wireless weather station that we mounted on a mast located about 30 metres away from the transmitting antennas. Internally, the weather station samples the relevant weather parameters every few seconds. Once per minute, it logs the average values of these parameters over the previous minute to an internal database. We used a custom software tool to match the received signal strength time series collected at a given location to the relevant weather data. Because previous work has shown that variations in average wind speed at tree top level or above are well correlated over mesoscale distances of several kilometers [27], we concluded that collecting wind data at a single location near the base station would be adequate for our purposes.

D. *Test Area*

Our transmitting antennas were installed atop the eighteen-storey office tower at BC Hydro's Edmonds facility in Burnaby, BC at a height of 80 m above ground level. The test area consisted of suburban neighbourhoods with generally flat terrain, light to moderate foliage and one- and two-storey houses. We collected measurement data at 92 fixed measurement locations that were situated within an annular sector between 1 and 4 km from the transmitter site. Almost all the motion in the environment arose from windblown foliage; few, if any, cars, people or other moving scatterers were in the vicinity of the receiver when we collected measurement data. Most of the foliage in the area is deciduous and between 4 and 7 m in height but at least one-third is coniferous and up to 15 m in height.

E. *Scope and Limitations*

Due to the nature of our measurement setup, our results apply strictly to suburban macrocell environments with high transmitting sites and moderate foliage. Development of a broadly applicable model will require additional data collected at other sites with transmitters at other heights. The duration of the measurement campaign was too short to permit observation of the effects of seasonal variations in the foliage. All of our data was collected with leaves on the trees.

In many fixed wireless deployments, the terminal antennas are directional. Because our primary objective is to compare the behaviour of the channel at different frequencies, we elected to simplify the data collection protocol by collecting the measurement data using omnidirectional antennas. If the remote terminal antenna's beamwidth decreased or its height increases, previous work suggests that the path gain and/or the Ricean K-factor will also tend to increase [7].

F. *Data Collection Protocol*

Our data collection protocol comprised the following steps. First, we conducted a rapid survey of the proposed measurement locations in order to ensure that the strength of

the received signal would be adequate at all locations. Next, over a span of several days, the operator drove the propagation measurement van to each of the fixed measurement locations that we had selected in advance. At each location, the operator collected simultaneous time series of the received strength of the 220, 850 and 1900 MHz CW signals. The measured data were collected in the form of fifteen successive 24-second sweeps. For the two higher bands, the pair of Anritsu MS2651B spectrum analyzers were used to record fifteen sweeps of 501 samples each, yielding 7515 received signal strength samples at each location and a sampling rate of 20.9 samples/sec. For the 220 MHz band, the Anritsu MS2721A spectrum analyzer was used; it yielded 551 samples per sweep or 8265 samples at each location and a sampling rate of 23.0 samples/sec. The sampling rates were chosen to be far greater than the anecdotal estimates of the maximum observed Doppler frequency reported previously, *e.g.*, [28],[29]. As reported in the next section, our estimates of the effective maximum Doppler frequency, which is always less than the maximum observed Doppler frequency, were all significantly lower than 10 Hz.

V. Results

A. Estimation of the Effective Maximum Doppler Frequency

We processed the time series data that we collected at 92 locations as follows: First, we estimated K using (3) and the zero-crossing rate ZCR, which is defined as the value of LCR for $\rho = 1$. This corresponds to the case where the threshold is equal to the mean value of the fading envelope. If $K > 3$, we estimated the effective maximum Doppler frequency f_d using (7). Otherwise, we estimated f_d using (6). We assessed the accuracy of the results by substituting our estimates of K and f_d into (4) and (5) to yield the theoretical LCR and AFD distributions, respectively, and then superimposing them on the corresponding LCR and AFD distributions obtained by directly processing the time series. This allowed us to determine how transient signal fading, transient signal enhancement and non-stationary channel behaviour affect the performance of the estimator, an issue not considered in [13].

An example where the theoretical and experimental AFD and LCR distributions are a close match is given in Figure 2. Reduction of time series data collected in the 850 MHz band at a distance of 1555 m from the base station yielded $K = 7.9$ dB and $f_d = 0.47$ Hz. Inspection of the time series suggests that both the depth and rate of fading is consistent across the 6-minute duration of the observation. We conclude that the model given by (4) applies. A counterexample where the theoretical and experimental AFD and LCR curves do not match particularly well is given in Figure 3. Reduction of time series collected in the 220 MHz band at a distance of 3170 m yielded $K = 33$ dB and $f_d = 1.30$ Hz. However, inspection of the time series reveals that the depth and rate of fading are not consistent across the duration of the observation. Instead, the signal is virtually flat for the first 100 seconds (with the exception of a brief fade and enhancement at $t = 80$ seconds) then begins to experience rapid and consistent scintillation during the remainder of the observation. We interpret this as a transition between two channel states.

We produced plots of individual time series and the

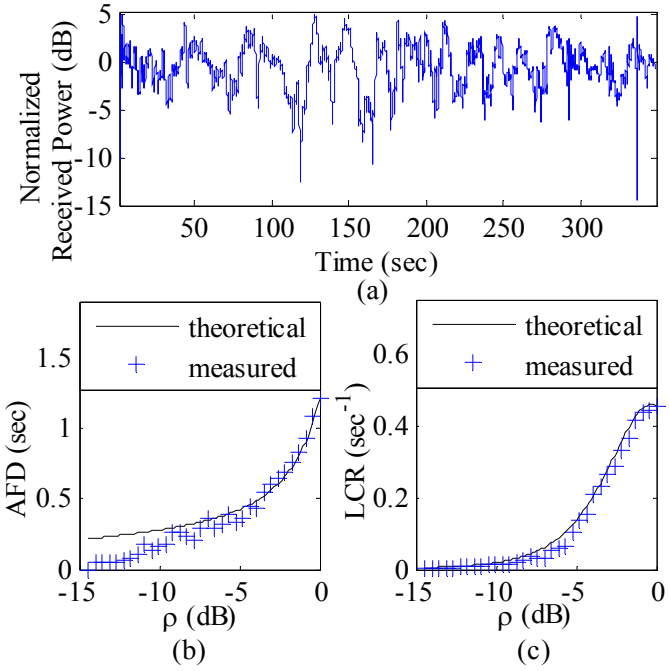

Fig. 2. A good fit between theoretical and measured fading distributions for: (a) Measured time series, (b) Average fade duration (AFD), and (c) Level crossing rate (LCR), where ρ is the threshold normalized to the rms envelope.

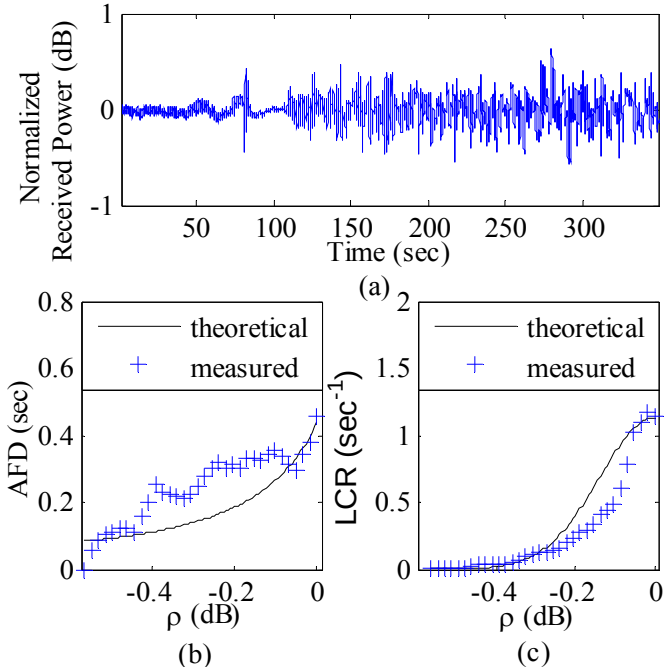

Fig. 3. A poor fit between theoretical and measured fading distributions for: (a) Measured time series, (b) Average fade duration (AFD), and (c) Level crossing rate (LCR), where ρ is the threshold normalized to the rms envelope.

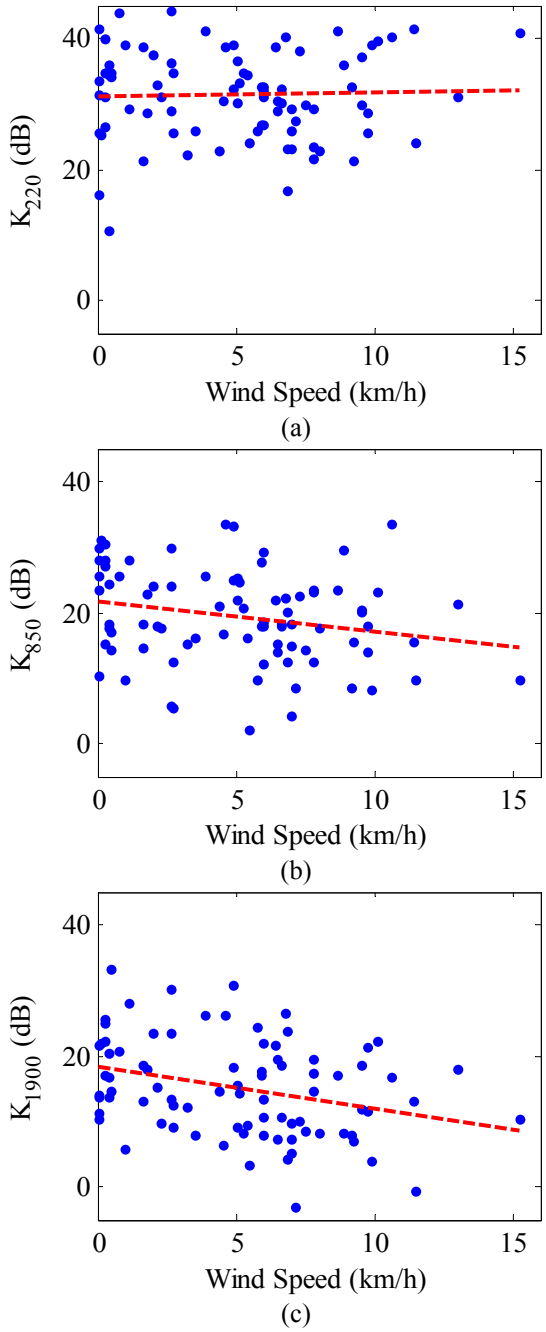

Fig. 4. Ricean K-factors observed at (a) 220 MHz, (b) 850 MHz and (c) 1900 MHz vs. average wind speed.

corresponding AFD and LCR distributions similar to those presented in Figure 2 and Figure 3 for all of our measurement locations. Deviations from stationary Ricean fading were identified by discrepancies between the empirical and theoretical AFD and LCR curves exist due to changes in channel state during the observation period. These deviations are quite obvious and easily discernable by visual inspection of both the AFD and LCR curves and the original RSSI time series data. The results are summarized in Table II. In the vast majority of cases (69% at 220 MHz, 75% at 850 MHz, and 85% at 1900 MHz), the depth and rate of fading in the time series were consistent across the duration of the observation and the theoretical and experimental curves matched well. Transient signal enhancement, possibly due to reflections from passing vehicles, was the most common impairment. Slow fading superimposed upon an otherwise consistent fading signal was the next most common impairment. Neither of these was observed to be dependent on distance. Slow fading tended to occur more often when the channel experienced high values of K. This suggests that the slow fading was the direct result of fading of the fixed component of the signal. In both cases, the experimental AFD curves were far more affected by fading and enhancement of the signal and deviated far more from their theoretical counterparts than did the experimental LCR curves. Between 4 and 9% of the time series in each band displayed either single or multiple transitions between channel states. In such cases, even the experimental LCR curves tended to deviate significantly from their theoretical counterparts. Because the parameters estimated from such time series would not be meaningful, we did not process them further.

TABLE II
DATA QUALITY SUMMARY IN PERCENTAGES

Impairment	220 MHz	850 MHz	1900 MHz
None	69%	75%	85%
Slow Fades	9%	7%	10%
Transient Peaks	16%	9%	1%
Non-Stationary Fading	3%	3%	3%
Transition between States	3%	6%	1%

B. Significance of the Equivalent Maximum Doppler Frequency

If the remote terminal is in motion and scattering is two-dimensional and isotropic, the Doppler spectrum of the fading signal follows Clarke's model and f_d in (4) and (5) is given by

$$f_d = k\, f_{d,\max} \ , \tag{8}$$

where $k = 1$. If the scattering is non-isotropic and/or the terminal is not in motion, the shape of the Doppler spectrum will be quite different. During the calibration and validation protocol described in Section III-B, we determined the value of k that applies to various Doppler spectrum shapes. We found that as the fraction of energy in the high frequency portion of the spectrum decreases, so does k. In particular, the 6-dB classic, flat and rounded spectra described in [30] yielded $k = 0.91$, 0.74 and 0.58, respectively. Further work will be required to determine the corresponding relationship for spectra more typical of those observed in fixed wireless environments, *e.g.*, [14],[15].

C. Joint-Distribution of Equivalent Maximum Doppler Frequencies

Over the 92 measurement locations and in all three frequency bands, the effective maximum Doppler frequency

distributions are well approximated by lognormal distributions (*i.e.*, normal in dBHz). Therefore, these effective maximum Doppler frequency values at 220, 850, and 1900 MHz bands can be cast as a three-element vector of jointly random Gaussian processes which are completely specified by the means, standard variations, and mutual correlation coefficients.

The mean values of the effective maximum Doppler frequency at 220, 850, and 1900 MHz bands are 1.62, 2.46, and 0.34 dBHz (or 1.45, 1.76, and 1.08 Hz, respectively.) The standard deviations of the effective maximum Doppler frequency in these bands are 2.03, 2.99 and 2.87 dBHz, respectively. The correlation matrix between the Doppler frequencies observed in these bands is given by

$$\rho = \begin{bmatrix} 1 & 0.63 & 0.61 \\ 0.63 & 1 & 0.64 \\ 0.61 & 0.64 & 1 \end{bmatrix} \tag{9}$$

where the rows and columns correspond to the bands in the sequence given above. It is apparent that the marginal distributions of the effective maximum Doppler frequencies are very similar among the three frequency bands. In particular, the rate of signal fading is not proportional to carrier frequency, as a simplistic model involving moving scatterers might suggest, *e.g.*, [14]. This constraint will provide useful guidance to those who seek to develop detailed physical models of fade dynamics on fixed wireless channels in suburban macrocell environments.

D. Ricean K-factor and Equivalent Maximum Doppler Frequency vs. Average Wind Speed

From previous work, it is well known that the Ricean K-factor drops as the average wind speed increases. However, the corresponding relationship between the effective maximum Doppler frequency and the average wind speed, and the effect of carrier frequency on the relationship between K and fd and the average wind speed has not been previously revealed. Our results for K and f_d vs. the average wind speed in the 220, 850 and 1900 MHz bands are presented in Figure 4 and Figure 5 respectively.

We estimated the regression line that best fits our measured data, the correlation coefficient between each parameter and the average wind speed, and the location variability of the parameter, *i.e.*, the variation of the parameter about the regression line at a given average wind speed. A regression line is the simplest model and, in the absence of a clear indication to the contrary, is a reasonable first choice when evaluating the relationship between two parameters. For completeness, we also evaluated the goodness of fit of a quadratic polynomial in each case but did not observe any improvement.

The regression line for K and f_d, and the corresponding correlation coefficients ρ and location variabilities σ in each frequency band are given by

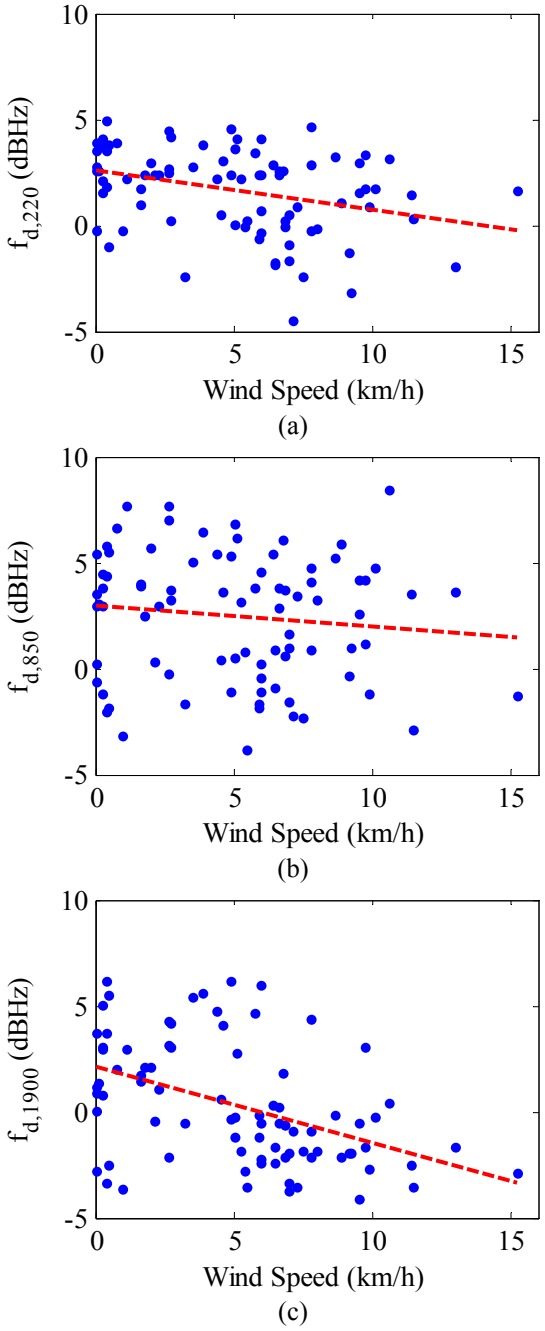

Fig. 5. Effective maximum Doppler frequency observed at (a) 220 MHz, (b) 850 MHz and (c) 1900 MHz vs. average wind speed.

$$\overline{K}_{220}(\text{dB}) = 0.066 v_W + 31.0; \quad \rho = 0.03,\ \sigma = 6.8 \text{ dB} \tag{10}$$

$$\overline{K}_{850}(\text{dB}) = -0.47 v_W + 21.7; \quad \rho = -0.23,\ \sigma = 7.0 \text{ dB} \tag{11}$$

$$\overline{K}_{1900}(\text{dB}) = -0.64 v_W + 18.42; \quad \rho = -0.31,\ \sigma = 7.0 \text{ dB} \tag{12}$$

and

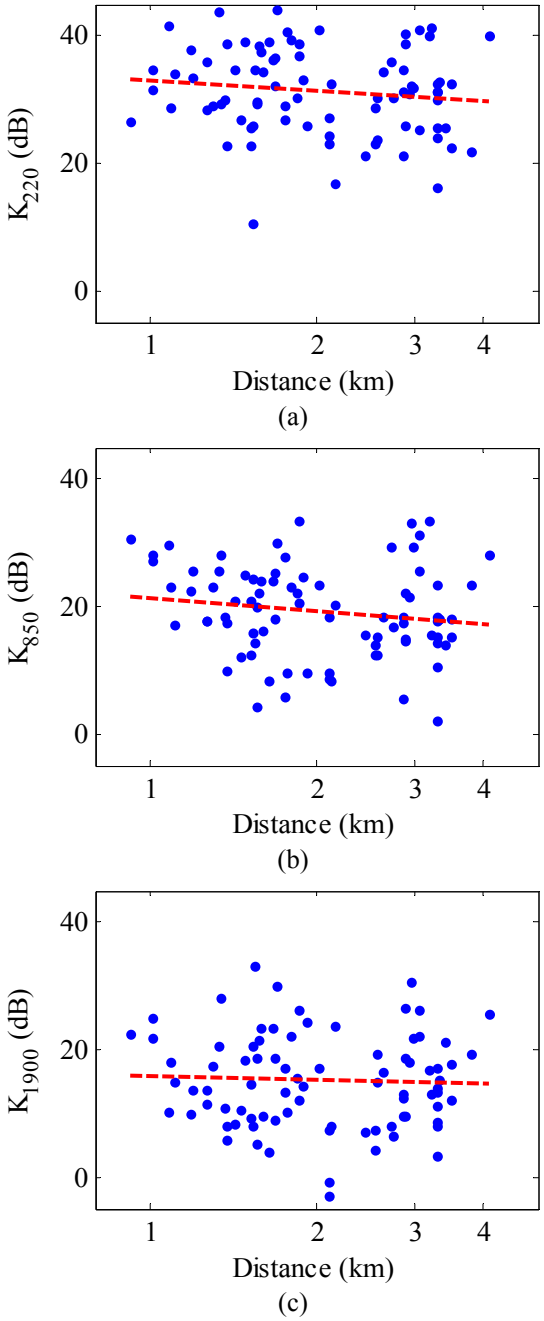

Fig. 6. Ricean K-factors observed at (a) 220 MHz, (b) 850 MHz and (c) 1900 MHz vs. distance.

$$\overline{f_{d\,220}}(\text{dBHz}) = -0.18 v_W + 2.56; \quad \rho = -0.32,\ \sigma = 1.9 \text{ dBHz} \tag{13}$$

$$\overline{f_{d\,850}}(\text{dBHz}) = -0.096 v_W + 2.95; \quad \rho = -0.11,\ \sigma = 3.0 \text{ dBHz} \tag{14}$$

$$\overline{f_{d\,1900}}(\text{dBHz}) = -0.36 v_W + 2.17; \quad \rho = -0.45,\ \sigma = 2.6 \text{ dBHz} \tag{15}$$

respectively, where the average wind speed, v_W , is expressed in km/h. In general, both K and f_d are weakly but negatively correlated with the average wind speed in all three bands. Here, we say that the correlation is weak if the mean value of ρ is less than 0.3. We say that no correlation exists if ρ = 0 occurs in the interval within one standard deviation from the mean of rho. In the 220 MHz band, K and the average wind speed are effectively uncorrelated.

E. Ricean K-factor and Equivalent Maximum Doppler Frequency vs. Distance

From previous work, it is well known that the Ricean K-factor tends to present a slight negative correlation with distance. However, the corresponding relationship between the effective maximum Doppler frequency and distance, and the effect of carrier frequency on the relationship between K and f_d and distance has not been previously revealed. Our results for K and f_d vs. distance in the 220, 850 and 1900 MHz bands are presented in Figure 6 and Figure 7 respectively.

We estimated the regression line that best fits our measured data, the correlation coefficient between each parameter and the distance, and the location variability of the parameter, *i.e.*, the variation of the parameter about the regression line at a given distance. The regression line for K and f_d and the corresponding correlation coefficients ρ and location variabilities σ in each frequency band are given by

$$\overline{K}_{220}(\text{dB}) = -5.8\log_{10} d + 33.2; \quad \rho = -0.14,\ \sigma = 6.7 \text{ dB} \tag{16}$$

$$\overline{K}_{850}(\text{dB}) = -6.8\log_{10} d + 21.4; \quad \rho = -0.16,\ \sigma = 7.1 \text{ dB} \tag{17}$$

$$\overline{K}_{1900}(\text{dB}) = -1.83\log_{10} d + 15.7; \quad \rho = -0.04,\ \sigma = 7.4 \text{ dB} \tag{18}$$

and

$$\overline{f_d}_{220}(\text{dBHz}) = -1.9\log_{10} d + 2.2; \quad \rho = -0.16,\ \sigma = 2.0 \text{ dBHz} \tag{19}$$

$$\overline{f_d}_{850}(\text{dBHz}) = -1.4\log_{10} d + 2.90; \quad \rho = -0.08,\ \sigma = 3.0 \text{ dBHz} \tag{20}$$

$$\overline{f_d}_{1900}(\text{dBHz}) = 0.53\log_{10} d + 0.18; \quad \rho = 0.03,\ \sigma = 2.9 \text{ dBHz} \tag{21}$$

respectively, where distance, d, is expressed in km. In general, neither K nor f_d are correlated with distance.

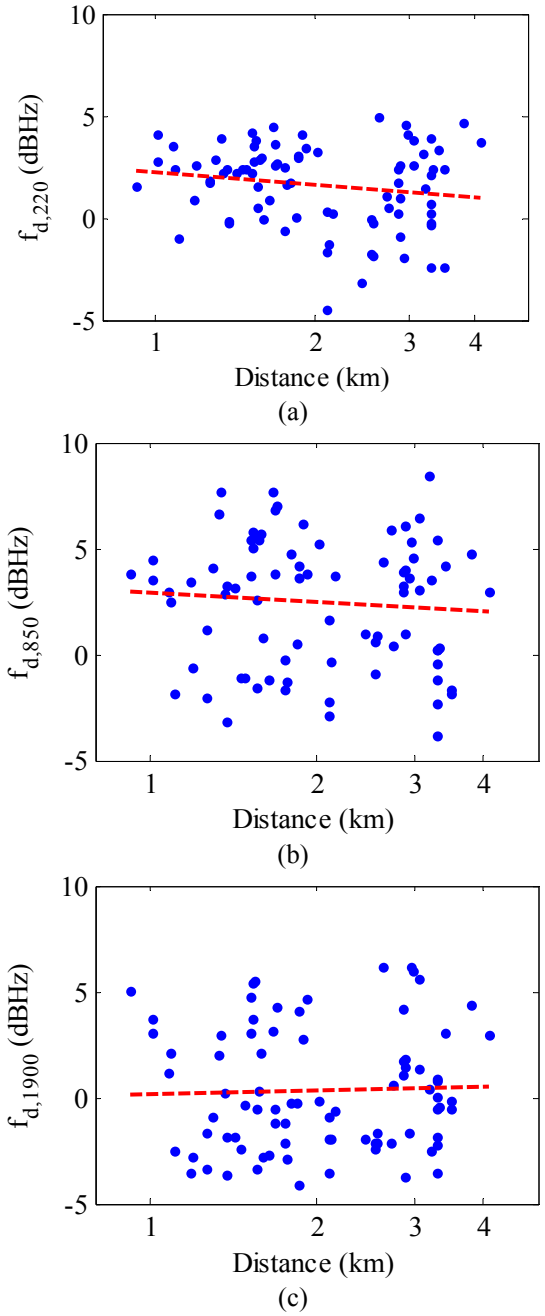

Fig. 7. Effective maximum Doppler frequencies observed at (a) 220 MHz, (b) 850 MHz and (c) 1900 MHz vs. distance.

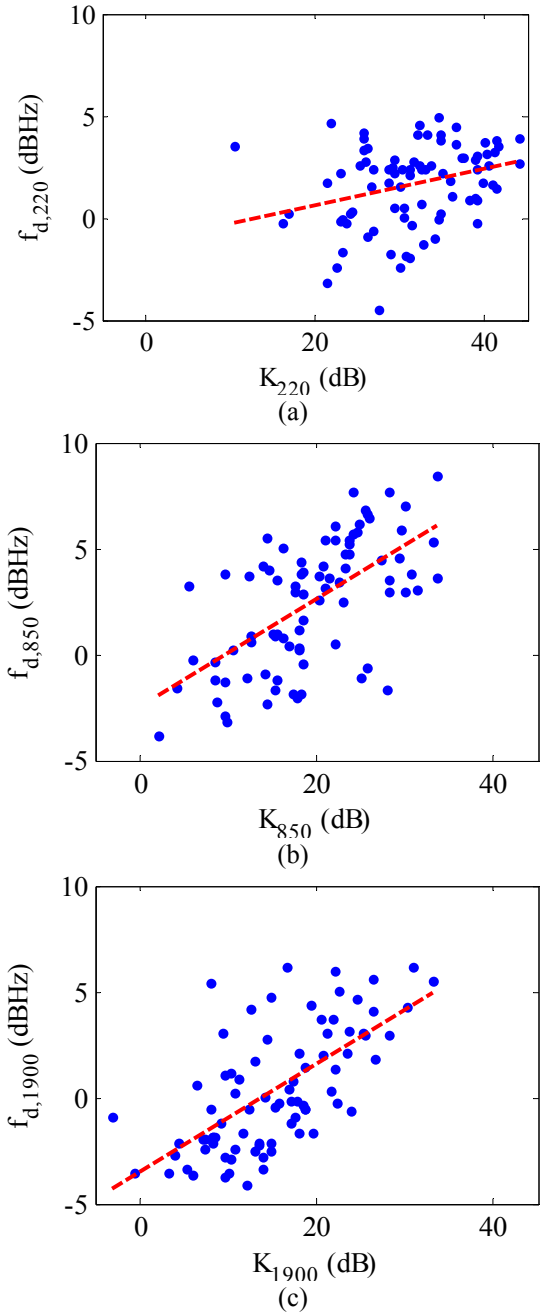

Fig. 8. Ricean K-factor vs. effective maximum Doppler frequency observed at (a) 220 MHz, (b) 850 MHz and (c) 1900 MHz.

F. *Joint Dependency of the Ricean K-factor and Equivalent Maximum Doppler Frequency*

We found that the Ricean K-factor (in dB) and the effective maximum Doppler frequency (in dBHz) both present normal distributions. This suggests that the two may be cast as jointly Gaussian random variables with specified mean, standard deviation and mutual correlation coefficient. Scatter plots of K and f_d in the 220, 850 and 1900 MHz bands are presented in Figure 8 together with the corresponding regression lines and correlation coefficients given by

$$\overline{f_{d\,220}}(\text{dBHz}) = 0.089\overline{K}_{220}(\text{dB}) - 1.18;\ \rho = 0.3 \qquad (22)$$

$$\overline{f_{d\,850}}(\text{dBHz}) = 0.26\overline{K}_{850}(\text{dB}) - 2.48;\ \rho = 0.62 \qquad (23)$$

$$\overline{f_{d\,1900}}(\text{dBHz}) = 0.26\overline{K}_{1900}(\text{dB}) - 3.56;\ \rho = 0.66 \qquad (24)$$

that best fit the data in a least-squares sense. The mean and standard deviations of K (in dB) in the 220, 850 and 1900 MHz bands are given by

$$\overline{K} = [31.4\ \text{dB} \quad 19.3\ \text{dB} \quad 15.2\ \text{dB}] \qquad (25)$$

$$\sigma_K = [6.8\ \text{dB} \quad 7.2\ \text{dB} \quad 7.4\ \text{dB}]. \qquad (26)$$

The corresponding mean and standard deviations of f_d are given in (19)-(21).

G. *Effect of Transmitter Height*

Although our measurement setup did not permit direct evaluation of the effect of transmitter height, physical reasoning suggests that as the transmitter height decreases, we can expect to see lower values of K due to a weaker direct signal and greater interaction with vegetation (*i.e.*, more scattering). However, we do not expect f_d to change because, although the magnitude of the fixed component is expected to increase, the physical process that leads to time variation does not change. Verification of these predictions is a task for future work.

H. *Physical Interpretation*

The results presented here tend to support a physical model proposed in [23] in which the vegetation mass may be considered as a diffraction aperture with a random aperture pattern. Although the objective of that work was to determine how changes in the random aperture due to wind blowing through leaves and branches affects the spatial distribution of fading at some distance beyond the vegetation mass, it can also be used to predict the effect of carrier frequency on both the depth and rate of fading. In particular, the model proposed in [23] correctly predicts that fading will be more severe at higher frequencies, but the rate of fading is strictly a function of the rate at which the random apertures open and close and not be dependent on the carrier frequency. Moreover, the results presented here suggest that the assumptions upon which the model is based apply well below 1 GHz. Detailed comparison of the model to measurement is a topic for future work.

VI. Conclusion

Our results corroborate Feick *et al.*'s observation [13] that even though the fixed Doppler spectrum assumes a much different shape than it does in mobility scenarios, substituting an appropriate value for what would normally be the maximum Doppler frequency (and which we refer to here as the effective maximum Doppler frequency) into the theoretical expressions for the LCR and AFD distributions often yields a good match to the fixed wireless observations.

Further, we have shown how transient peaks, fades, or non-stationary behaviour in the fading signal affect the fit of the measured LCR and AFD curves to their theoretical counterparts and have provided convincing evidence that

fitting the theoretical LCR curve to the measured curve provides the most robust and reliable results. Finally, we recount preliminary results that suggest that the ratio of the effective maximum Doppler frequency to the maximum Doppler frequency: (i) is determined by the shape of the Doppler spectrum and (ii) decreases as the fraction of energy in the high frequency components of the Doppler spectrum decreases.

Our most significant finding is that the effective maximum Doppler frequency observed at a given location is not proportional to the carrier frequency as: (i) a model based upon the radial motion of moving scatterers would predict and (ii) what others have observed in conventional indoor and mobility environments. This suggests that the random aperture model proposed in [23] is correct and is valid at frequencies below 1 GHz. Further, we found that the effective maximum Doppler frequency is effectively independent of either distance or average wind speed and is lognormally distributed about its mean value, which typically falls between 1 and 2 Hz. Although the lognormal distribution suggests that the randomness is the result of a multiplicative process, determining the precise details is a task for future work.

The results presented here will provide useful guidance to those who seek to: (i) simulate channels encountered in suburban macrocell environments with high transmitting sites and moderate foliage or (ii) develop detailed physical models of propagation in such environments. Although our test site is typical of suburban neighborhoods with light to moderate foliage, other sites that are not as homogenous or that have more or less vegetation may yield slightly different results. We believe it is unlikely that observations of the depth and rate of channel fading at other sites will show large deviations from the trends presented here, however, development of measurement-based models applicable to a broad range of environments will require additional data collected: (i) at other sites, (ii) with transmitters at different heights and (iii) at additional frequencies within the range of interest.

ACKNOWLEDGMENT

We thank BC Hydro Telecom Services for providing us with access to the radio room and rooftop facilities atop Edmonds tower that we used as our transmitting site. We also thank UBC Student Housing and Conferences for providing us with access to the Walter Gage Residence, East Tower during our equipment development and validation runs.

REFERENCES

[1] W. Webb, "Broadband fixed wireless access as a key component of the future integrated communications environment," *IEEE Commun. Mag.,* vol. 39, no. 9, pp. 115-121, Sep. 2001.

[2] K. Lu, Y. Qian and H-H Chen, "Wireless broadband access: WIMAX and beyond," *IEEE Commun. Mag*., vol. 45, no. 5, pp. 124-130, May 2007.

[3] S. S. Venkata, A. Pahwa, R. E. Brown, and R. D. Christie, "What future distribution engineers need to learn," *IEEE Trans. Power Syst.*, vol.19, no.1, pp. 17-23, Feb. 2004.

[4] G. Simard and D. Chartrand, "Hydro-Quebec's Economic and Technical Approach to Justify its Distribution Automation Program," in *Proc. IEEE PES'07,* pp. 1-5, 24-28 Jun. 2007.

[5] S. Jim, W. Carr, and S. E. Collier, "Real time distribution analysis for electric utilities," in *Proc. IEEE REPC'08,* pp. B5-B5-8, 27-29 Apr. 2008.

[6] D. G. Michelson, V. Erceg, and L. J. Greenstein, "Modeling diversity reception over narrowband fixed wireless channels," in *Proc. IEEE MTT-TWA'99*, pp. 95-100, 21-24 Feb. 1999.

[7] L. J. Greenstein, S. S. Ghassemzadeh, V. Erceg and D. G. Michelson, "Ricean K-factors in narrowband fixed wireless channels: Theory, experiments and statistical models," in *Proc. WPMC'99*, 21-23 Sep. 1999.

[8] S. Perras and L. Bouchard, "Fading characteristics of RF signals due to foliage in frequency bands from 2 to 60 GHz," in *Proc. WPMC'02*, 27-30 Oct. 2002, pp. 267-271.

[9] M. J. Gans, N. Amitay, Y. S. Yeh, T. C. Damen, R. A. Valenzuela, C. Cheon and J. Lee, "Propagation measurements for fixed wireless loops (FWL) in a suburban region with foliage and terrain blockages," *IEEE Trans. Wireless Commun.*, vol. 1, no. 2, pp. 302-310, Apr. 2002.

[10] E. R. Pelet, J. E. Salt, and G. Wells, "Effect of wind on foliage obstructed line-of-sight channel at 2.5 GHz," *IEEE Trans. Broadcasting*, vol. 50, no. 3, pp. 224-232, 2004.

[11] D. Crosby, V. S. Abhayawardhana, I. J. Wassell, M. G. Brown, and M. P. Sellars, "Time variability of the foliated fixed wireless access channel at 3.5 GHz," in *Proc. IEEE VTC 2005 Spring*, 25-28 Sep. 2005, pp. 106-110.

[12] H. Suzuki, C. D. Wilson, and K. Ziri-Castro, "Time variation characteristics of wireless broadband channel in urban area," presented at *EuCAP'06*, Nice, France, 2-6 Nov. 2006.

[13] R. Feick, R. A. Valenzuela and L. Ahumada, "Experiment results on the level crossing rate and average fade duration for urban fixed wireless channels," *IEEE Trans. Commun.,* vol. 9, no. 1, pp. 175-179, Jan. 2007.

[14] S. Thoen, L. V. D. Perre, and M. Engels, "Modeling the channel time-variance for fixed wireless communications," *IEEE Communic. Lett.*, vol. 6, no. 8, pp. 331-333, Aug. 2002.

[15] A. Domazetovic, L. J. Greenstein, N. B. Mandayam, and I. Seskar, "Estimating the Doppler spectrum of a short-ranged fixed wireless channel," *IEEE Communic. Lett.*, vol. 7, no. 5, pp. 227-229, May 2003.

[16] K. E. Baddour and N. C. Beaulieu, "Accurate simulation of multiple cross-correlated Rician fading channels," *IEEE Trans. Commun*. vol. 52, no. 11, pp. 1980-1987, Nov. 2004.

[17] B. Natarajan, C. R. Nassar and V. Chandrasekhar, "Generation of correlated Rayleigh fading envelopes for spread spectrum applications," *IEEE Communic. Lett*., vol. 4, no. 1, pp. 9-11, Jan. 2000

[18] "Policy for the Use of 700 MHz Systems for Public Safety Applications and Other Limited Use of Broadcasting Spectrum," Industry Canada Radio Systems Policy, RP-006 – Issue 1, Jun. 2006.

[19] "Proposals and Changes to the Spectrum in Certain Bands below 1.7 GHz," Industry Canada Gazette Notice DGTP-004-05, Dec. 2005.

[20] M. Hata, "Empirical formula for propagation loss in land mobile radio services," *IEEE Trans. Veh. Technol.,* vol. 29, no. 3, pp. 317-325, Aug. 1980.

[21] E. Damosso, Ed., "Digital Mobile Radio Toward Future Generation Systems - Final Report," COST 231 Final Report, 1996.

[22] V. Erceg, L. J. Greenstein, S. Y. Tjandra, S.R. Parkoff, A. Gupta, B. Kulic, A. A. Julius, and R. Bianchi, "An empirically based path loss model for wireless channels in suburban environments," *IEEE J. Sel. Areas Commun.,* vol. 17, no. 7, pp. 1205-1211, July 1999.

[23] D. A. J. Pearce, A. G. Burr and T. C. Tozer, "Modelling and predicting the fading performance of fixed radio links through vegetation," in *Proc. IEE NCAP'99,* 31 Mar.-1 Apr. 1999, pp. 263-266.

[24] P. Lédl, P. Pechač and M. Mazánek, "Time-series prediction of attenuation caused by trees for fixed wireless access systems operating in millimeter waveband," in *Proc. IEE ICAP'03,* 31 Mar.-3 Apr. 2003, pp. 646-649.

[25] M. Cheffena and T. Ekman, "Modeling the dynamic effects of vegetation on radiowave propagation," in *Proc. IEEE ICC'08*, 19-23 May 2008, pp. 4466-4471.

[26] L. J. Greenstein, D. G. Michelson, and V. Erceg, "Moment-method estimation of the Ricean K-factor," *IEEE Commun. Lett,* vol. 3, no. 6, pp. 175-176, Jun. 1999.

[27] S. R. Hanna and J. C. Chang, "Representativeness of wind measurements on a mesoscale grid with station separations of 312 m to 10 km," *Boundary-Layer Meteorol,* vol. 60, pp. 309-324, 1992.

[28] D. S. Baum, D. A. Gore, R. U. Nabar, S. Panchanathan, K. V. S. Hari, V. Erceg and A. J. Paulraj, "Measurements and characterization of broadband MIMO fixed wireless channels at 2.5 GHz," in *Proc. IEEE ICPWD'00,* 17-20 Dec. 2000, pp. 203-206.

[29] V. Erceg et al., "Channel models for fixed wireless applications," IEEE 802.16 Broadband Wireless Access Working Group, IEEE 802.16a-03/01, 27 Jun. 2003.

[30] "SR5500 Wireless Channel Emulator Operations Manual," Spirent Communications, Eatontown, NJ, 2006, pp. 3-16.

Kyle N. Sivertsen received the B.A.Sc. degree in electrical engineering from the University of British Columbia (UBC), Vancouver, BC, Canada in 2007. He is currently a M.A.Sc. candidate with the Department of Electrical and Computer Engineering, UBC.

His main research interests include propagation and channel modeling for fixed wireless communications.

Anthony Liou received the B.A.Sc. and M.A.Sc. degrees in electrical engineering from the University of British Columbia (UBC), Vancouver, BC, Canada in 2006 and 2009, respectively. His thesis project focused on propagation and channel modeling for fixed wireless communications.

He recently joined Universal Scientific Industrial Co., Taiwan where he is working as an engineer-in-training within the RF branch.

David G. Michelson (S'80–M'89–SM'99) received the B.A.Sc., M.A.Sc., and Ph.D. degrees from the University of British Columbia (UBC), Vancouver, BC, Canada, all in electrical engineering.

From 1996-2001, he served as a member of a joint AT&T Wireless Services (Redmond, WA) and AT&T Labs – Research (Red Bank, NJ) team concerned with development of propagation and channel models for next generation and fixed wireless systems. The results of this work formed the basis for the propagation and channel models later adopted by the IEEE 802.16 Working Group on Broadband Fixed Wireless Access Standards. From 2001-2002, he helped to oversee deployment of one of the world's largest campus wireless LANs at the University of British Columbia while also serving as an adjunct professor in the Department of Electrical and Computer Engineering. Since 2003, Prof. Michelson has led the Radio Science Lab at UBC where his current research interests include propagation and channel modeling for fixed wireless, UWB and satellite communications.

Professor Michelson serves as Chair of the IEEE VT-S Technical Committee on Propagation and Channel Modeling, as an Associate Editor for Mobile Channels for IEEE Vehicular Technology Magazine and as an Editor for IEEE Transactions on Wireless Communications. From 1999-2007, he chaired the IEEE Vancouver Section's Joint Communications Chapter. Under his leadership, the Chapter received Outstanding Achievement Awards from the IEEE Communications Society in 2002 and 2005, and the Chapter of the Year Award from IEEE Vehicular Technology in 2006. He received the E.F. Glass Award from IEEE Canada in 2009 and currently serves as Chair of Vancouver Section. Under his leadership, the Section received the Outstanding Section Award from IEEE Canada in 2010.